Double-Quantum Filtration under Rotational-Resonance Conditions: Numerical Simulations and Experimental Results

Stephan Dusold and Angelika Sebald[1]

Bayerisches Geoinstitut, Universität Bayreuth, D-95440 Bayreuth, Germany

E-mail: stephan@dusold.de, angelika.sebald@uni-bayreuth.de

The dependence of the performance of a recently introduced pulse sequence to achieve double-quantum excitation under the $n = 1$ rotational-resonance condition (T. Karlsson, M. Edén, H. Luthman, and M. H. Levitt, 2000, *J. Magn. Reson.* 145, 95–107) on different spin-system properties is investigated by means of numerical simulations and ^{13}C MAS NMR experiments. For spin systems where chemical shielding anisotropies amount to only an insignificant fraction of the isotropic chemical shielding difference, high efficiencies are found for large and small dipolar coupling interactions. In the presence of significant chemical shielding anisotropies the overall efficiencies decrease and become strongly dependent on the duration of the excitation period. It is demonstrated that those spin-system parameters which are sensitively encoded in the lineshapes of a conventional $n = 1$ rotational-resonance spectrum are similarly sensitively encoded in the corresponding rotational-resonance double-quantum-filtered lineshapes and may be quantitatively recovered by iterative lineshape-fitting approaches. In certain favorable circumstances, the in-built selectivity of the rotational-resonance double-quantum-filtration approach permits successful application of the experiment on spin systems with more than two spins. © 2000 Academic Press

Key Words: MAS NMR; rotational resonance; double-quantum filtration; numerical simulations; ^{13}C spin systems.

INTRODUCTION

Among the numerous solid-state NMR techniques designed to restore homo- or heteronuclear dipolar coupling interactions under magic-angle spinning (MAS), the so-called rotational-resonance (R^2) MAS NMR condition (*1–7*) for homonuclear spin systems holds a rather special position. R^2 recoupling does not require application of RF pulses but occurs at specific MAS frequencies matching the difference in isotropic chemical shielding between two spins ($\omega_{iso}^{\Delta} \approx n\omega_r$, where n is a small integer). Under R^2 conditions all anisotropic interactions are recoupled and the condition $\omega_{iso}^{\Delta} \approx n\omega_r$ lends some in-built selectivity to the experimentally straightforward R^2 MAS NMR experiment. The literature provides ample evidence for the successful application of R^2 MAS NMR experiments in the determination of internuclear distances and chemical shielding tensor orientations, as well as modifications of the basic R^2 MAS NMR experiment aiming at the determination of larger internuclear distances or improvements of the selectivity (*8*). The key to the wealth of information encoded in conventional R^2 MAS NMR experiments, however, is the presence of spatially isolated spin systems in the sample, either naturally occurring or prepared by selective isotope enrichment. These requirements often represent serious limitations for the applicability of conventional R^2 MAS NMR techniques and call for experimental alternatives, providing efficient double-quantum filtration (DQF) under R^2 conditions. Pathways for double-quantum excitation under R^2 conditions could be either indirect dipolar (*J* coupling) or direct dipolar coupling. While the *J*-coupling path has been successfully exploited for this purpose under MAS conditions (*9–14*), in the context of MAS NMR the usually more relevant coupling path is direct dipolar coupling. Very recently, a pulse sequence which achieves double-quantum excitation *via* direct dipolar coupling under the $n = 1$ R^2 condition has been introduced (*15*). This R^2-DQF pulse sequence features a series of simple three-pulse subsequences and does not require rotation synchronization. Hence, this pulse sequence is expected to be experimentally robust to implement and promises to be applicable also for samples with chemically problematic properties. The dependence of the performance of this pulse sequence on various properties of isolated two-spin systems and of multispin systems is investigated in the following. Our investigation employs numerical simulations in conjunction with experiments on two model compounds (Fig. 1): different ^{13}C isotopomers of sodium pyruvate, **1,** provide isolated two- and three-^{13}C-spin systems, while L-tyrosine-ethylester, **2,** in its fully ^{13}C-enriched form (**2-U^{13}C**) provides a realistic testing ground for the performance in true multiple-^{13}C-spin systems. The crystal structures of **1** (*16*) and **2** (*17*) are known.

---

[1] To whom correspondence should be addressed.

$$CH_3-\underset{\underset{O}{\|}}{C}-CO_2 \,^{-}\, Na^+$$

1

$$HO-\overset{(2)\quad(3)}{\underset{(6)\quad(5)}{\bigcirc}}-\overset{(7)}{CH_2}-\overset{(8)}{\underset{\underset{NH_2}{|}}{CH}}-\overset{\overset{O}{\|}}{\underset{(9)}{C}}-O-\overset{(10)}{CH_2}-\overset{(11)}{CH_3}$$
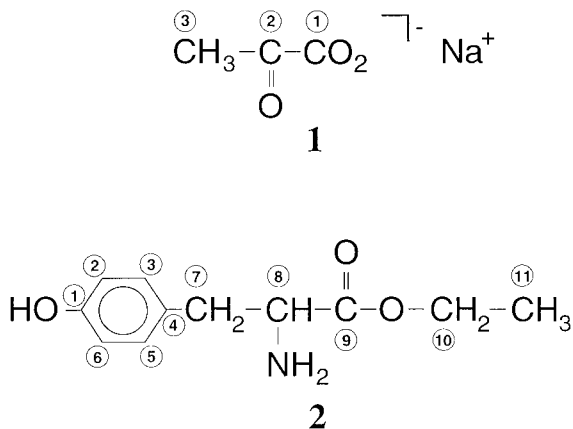
2

FIG. 1. Schematic representation of the molecular structures of **1** and **2**. The numbering of the carbon atoms is identical to the numbering schemes used in the description of the respective X-ray diffraction structures of **1** (*16*) and **2** (*17*) and will be used throughout.

EXPERIMENTAL

Samples

The sodium pyruvate samples used in this study are commercially available (**1**, with ^{13}C in natural abundance (Aldrich Chemicals); **1-C1/C2,** selectively $^{13}C1$, $^{13}C2$-enriched sodium pyruvate; **1-C2/C3,** selectively $^{13}C2$, $^{13}C3$-enriched sodium pyruvate; and **1-U^{13}C,** fully ^{13}C-enriched sodium pyruvate (Isotec Inc.)) and were used as received. Our sample of fully ^{13}C-enriched L-tyrosine-ethylester (**2-U^{13}C**) was provided by C. Hoffmann and C. Griesinger, Frankfurt.

^{13}C MAS NMR

^{13}C MAS NMR spectra were recorded on Bruker MSL 100, MSL 200, DSX 400, and DSX 500 NMR spectrometers. The corresponding ^{13}C Larmor frequencies $\omega_0/2\pi$ are -25.2, -50.3, -100.6, and -125.8 MHz. ^{13}C chemical shielding is quoted with respect to $\omega_{iso}^{CS} = 0$ ppm for the ^{13}C resonance of $SiMe_4$. MAS frequencies were generally in the range $\omega_r/2\pi = 1–18$ kHz and were actively controlled to within ±2 Hz. Lineshapes of experimental ^{13}C MAS NMR spectra were checked to be identical when using either Hartmann–Hahn cross polarization (CP) or ^{13}C single-pulse excitation. ^{13}C R^2 MAS NMR spectra for purposes of lineshape fitting were recorded on the DSX 400 and DSX 500 NMR spectrometers with TPPM (*18*) ^1H decoupling with amplitudes of 83–105 kHz applied during signal acquisition. ^{13}C R^2-DQF MAS NMR experiments (*15*) were carried out on the MSL 100 (7-mm-o.d. ZrO_2 rotor, ^{13}C $\pi/2$ pulse duration 4.0 μs, cw ^1H decoupling amplitudes of 62.5 kHz) and MSL 200 (4-mm-o.d. ZrO_2 rotor, ^{13}C $\pi/2$ pulse duration 3.0 μs, cw ^1H decoupling amplitudes of 83.3 kHz) NMR spectrometers.

The pulse sequence of the recently introduced R^2-DQF MAS NMR experiment (*15*) is depicted in Fig. 2. This version of the experiment is suitable for the $n = 1$ R^2 condition and inverts the less shielded resonance of a spin pair. The general working of the pulse sequence is step-by-step fully explained in Ref. (*15*). In brief, the R^2-DQF pulse sequence excites DQ coherence by making use of R^2 echoes. First, cross polarization creates transverse magnetization of the observed spins, which is transformed into longitudinal difference magnetization by the first three-pulse sequence. This longitudinal difference magnetization is converted into zero-quantum coherence under the influence of the homonuclear dipolar coupling, recoupled by R^2. The second three-pulse sequence excites DQ coherence, which is reconverted to zero-quantum coherence by the subsequent third three-pulse sequence. During the following interval the zero-quantum coherence is converted back to longitudinal magnetization, which forms an echo at time point 5, where a strong nonselective $\pi/2$ read-out pulse is applied. Appropriate phase cycling (*15*) selects the signal that has passed through DQ coherence at time point 3 (see Fig. 2).

Definitions, Notation, and Numerical Methods

Shielding notation (*19*) is used throughout. For the interactions $\lambda = CS$ (chemical shielding), $\lambda = D$ (direct dipolar coupling), and $\lambda = J$ (indirect dipolar (J) coupling) the isotropic part ω_{iso}^{λ}, the anisotropy δ^{λ}, and the asymmetry parameter η^{λ} relate to the principal elements of the interaction tensor ω^{λ} as follows (*20*): $\omega_{iso}^{\lambda} = (\omega_{xx}^{\lambda} + \omega_{yy}^{\lambda} + \omega_{zz}^{\lambda})/3$, $\delta^{\lambda} = \omega_{zz}^{\lambda} - \omega_{iso}^{\lambda}$, and $\eta^{\lambda} = (\omega_{yy}^{\lambda} - \omega_{xx}^{\lambda})/\delta^{\lambda}$ with $|\omega_{zz}^{\lambda} - \omega_{iso}^{\lambda}| \geq |\omega_{xx}^{\lambda} - \omega_{iso}^{\lambda}| \geq |\omega_{yy}^{\lambda} - \omega_{iso}^{\lambda}|$. For indirect dipolar coupling $\omega_{iso}^{J} = \pi J_{iso}$, and for direct dipolar coupling $\eta^D = \omega_{iso}^D = 0$ and $\delta^{D_{ij}} = b_{ij} = -\mu_0\gamma_i\gamma_j\hbar/(4\pi r_{ij}^3)$, where γ_i, γ_j denote gyromagnetic ratios and r_{ij} is the internuclear distance between spins S_i, S_j. The Euler angles $\Omega_{IJ} = \{\alpha_{IJ}, \beta_{IJ}, \gamma_{IJ}\}$ (*21*) relate axis system I to axis system J, where I, J denote P (principal axis system, PAS), C (crystal axis system, CAS), R (rotor axis system, RAS), or L (laboratory axis system). For lineshape simulations of R^2 MAS NMR spectra of isolated two-spin systems (S_i, S_j)
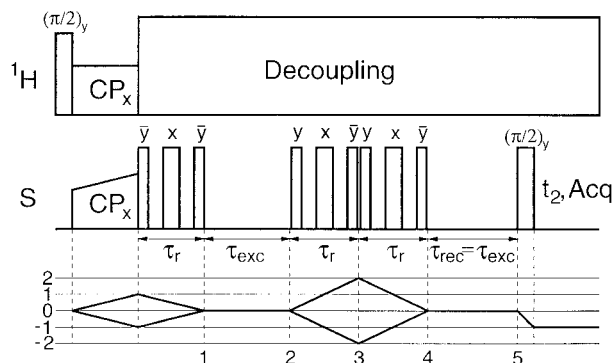
FIG. 2. The pulse sequence and coherence-transfer paths of the R^2-DQF MAS NMR experiment (*15*) with cross polarization. τ_r denotes the rotation period and the three-pulse sequences consist of equally spaced $\pi/4-\pi/2-\pi/4$ pulses.

it is convenient to define the PAS of the corresponding dipolar coupling tensor $\omega^{D_{ij}}$ as the CAS, $\Omega_{PC}^{D_{ij}} = \{0, 0, 0\}$. Our procedures for numerically exact spectral lineshape simulations and iterative fitting are fully described and discussed in detail elsewhere, in particular addressing the $n = 0$ R^2 condition for isolated homonuclear spin pairs (22) and various $n = 0, 1, 2$ R^2 conditions in an isolated homonuclear ^{13}C four-spin system (23). In general, these numerical procedures employ the REPULSION (24) or Lebedev (25) schemes for the calculation of powder averages, implement some of the routines of the GAMMA package (26), and use, where possible, the γ-COMPUTE approach (27–30). The pulse sequence of the R^2-DQF experiment (15) is not synchronous with the MAS rotation period and simulation of the underlying spin dynamics hence requires application of the so-called direct method for the calculation of the time evolution. Direct-method simulations are ca. 30 to 100 times more time consuming than comparable simulations where γ-COMPUTE approaches can be employed.

RESULTS AND DISCUSSION

This section is organized into three parts as follows. In order to be able to evaluate the experimental performance of the R^2-DQF experiment (15) on a ^{13}C spin system with known properties, we first determine the parameters of the ^{13}C spin system in sodium pyruvate by means of iterative lineshape simulations of conventional ^{13}C R^2 MAS NMR spectra. Next, we investigate by numerical simulations the dependence of the performance of the R^2-DQF experiment on the properties of isolated two-spin systems; in addition we compare experimental results on the pyruvate ^{13}C spin system to numerical simulations. The third part deals with the R^2-DQF experiment applied to multiple-^{13}C-spin systems.

The ^{13}C Chemical Shielding Tensors in Sodium Pyruvate

A full description of the ^{13}C three-spin system in the pyruvate moiety requires knowledge of 30 parameters: $3 \cdot 6 = 18$

TABLE 1
^{13}C Chemical Shielding Tensors in Sodium Pyruvate

	$^{13}C1$	$^{13}C2$	$^{13}C3$
ω_{iso}^{CS} [ppm]	−168.2	−205.5	−28.7
δ^{CS} [ppm]	−82 ± 2	110 ± 2	24 ± 5
η^{CS}	0.5 ± 0.1	0.6 ± 0.1	0.7 ± 0.1
$\alpha_{PC_{12}}^{CS}$ [°][a]	60, 135 ± 20	0 ± 15	—[b]
$\beta_{PC_{12}}^{CS}$ [°][a]	0 ± 12	95 ± 2	—[b]
$\gamma_{PC_{12}}^{CS}$ [°][a]	0[c]	90 ± 5	—[b]

[a] Euler angles given relative to the principal axis system of the $^{13}C1$–$^{13}C2$ dipolar coupling tensor with its y axis defined as perpendicular to the molecular C1–C2–C3 plane.
[b] Not determined; see text.
[c] Arbitrarily chosen; see text.

TABLE 2
Direct and Indirect Dipolar ^{13}Ci–^{13}Cj Couplings in Sodium Pyruvate

	$ij = 12$	$ij = 13$	$ij = 23$
$b_{ij}/2\pi$ [Hz][a]	−2004	−430	−2259
$\omega_{ij}^{J_{iso}}$ [Hz][b]	+62.1	±13.5	+39.6

[a] Calculated from the known internuclear distances (16).
[b] Determined by solution-state ^{13}C NMR of an aqueous solution of **1-U^{13}C.**

CSA parameters, $3 \cdot 3 = 9$ dipolar coupling parameters, and $3 \cdot 1 = 3$ J-coupling parameters (if the anisotropy of $J(^{13}C, {}^{13}C)$ couplings is neglected). From the known structure of sodium pyruvate (16) the magnitudes and orientations of the three dipolar coupling tensors can be calculated; ^{13}C MAS NMR experiments on **1** (with ^{13}C in natural abundance) yield the magnitudes of the three ^{13}C CSA tensors, and solution-state ^{13}C NMR measurements on **1-U^{13}C** provide a good estimate of the three values $J_{iso}(^{13}C, {}^{13}C)$ (see Tables 1 and 2). With all this preliminary information available, 9 unknown parameters remain to be determined, that is, the Euler angles ($\alpha_{PC}^{CS_i}$, $\beta_{PC}^{CS_i}$, $\gamma_{PC}^{CS_i}$; $i = 1, 2, 3$) representing the orientation of the three ^{13}C CSA tensors in the molecular frame. The determination of these parameters by means of ^{13}C MAS NMR requires pairwise and/or fully ^{13}C-enriched sodium pyruvate samples and experimental ^{13}C MAS NMR conditions where the unknown orientational ^{13}C CSA parameters remain encoded in the spectral lineshapes. The differences in isotropic ^{13}C chemical shielding for solid sodium pyruvate are $\omega_{iso}^{\Delta_{12}} = 37.3$ ppm, $\omega_{iso}^{\Delta_{23}} = 176.8$ ppm, and $\omega_{iso}^{\Delta_{13}} = 139.5$ ppm. Accordingly, experimental ^{13}C R^2 MAS NMR spectra with $n = 1, 2, 3 \ldots$ of various ^{13}C sodium pyruvate isotopomers are accessible over a wide range of Larmor frequencies and can serve as the experimental data input for lineshape simulations.

With the PAS of the dipolar coupling tensor $\omega^{D_{12}}$ taken as the CAS C_{12}, R^2 MAS NMR spectra of the ^{13}C two-spin system in **1-C1/C2** should reflect the five Euler angles $\alpha_{PC_{12}}^{CS_{ij}}$, $\beta_{PC_{12}}^{CS_{ij}}$, $\gamma_{PC_{12}}^{CS_{i}}$ with $i, j = 1, 2$ and thus define the relative orientations of the $^{13}C1$ and $^{13}C2$ CSA tensors. Based on an experimental $n = 1$ ^{13}C R^2 MAS NMR spectrum of **1-C1/C2** with $\omega_0/2\pi = -100.6$ MHz and $\omega_r/2\pi = 3739$ Hz (see Fig. 3a), an initial search reveals that mainly the three angles $\alpha_{PC_{12}}^{CS_2}$, $\beta_{PC_{12}}^{CS_1}$, and $\beta_{PC_{12}}^{CS_2}$ are sensitive fit parameters (see Fig. 4). Calculation of the full three-dimensional error map for these three parameters yields a single well-defined minimum at $\alpha_{PC_{12}}^{CS_2} = 10°$, $\beta_{PC_{12}}^{CS_1} = 5°$, and $\beta_{PC_{12}}^{CS_2} = 95°$ (compare Table 1). With these three parameters fixed to their minimum values, subsequent calculation of the two-dimensional error map for the two remaining, less sensitive fit parameters $\alpha_{PC_{12}}^{CS_1}$ and $\gamma_{PC_{12}}^{CS_1}$ leads to several minima and shows $\alpha_{PC_{12}}^{CS_1}$ and $\gamma_{PC_{12}}^{CS_1}$ to be strongly correlated (see Fig. 5). We will reconsider these two parameters further below.

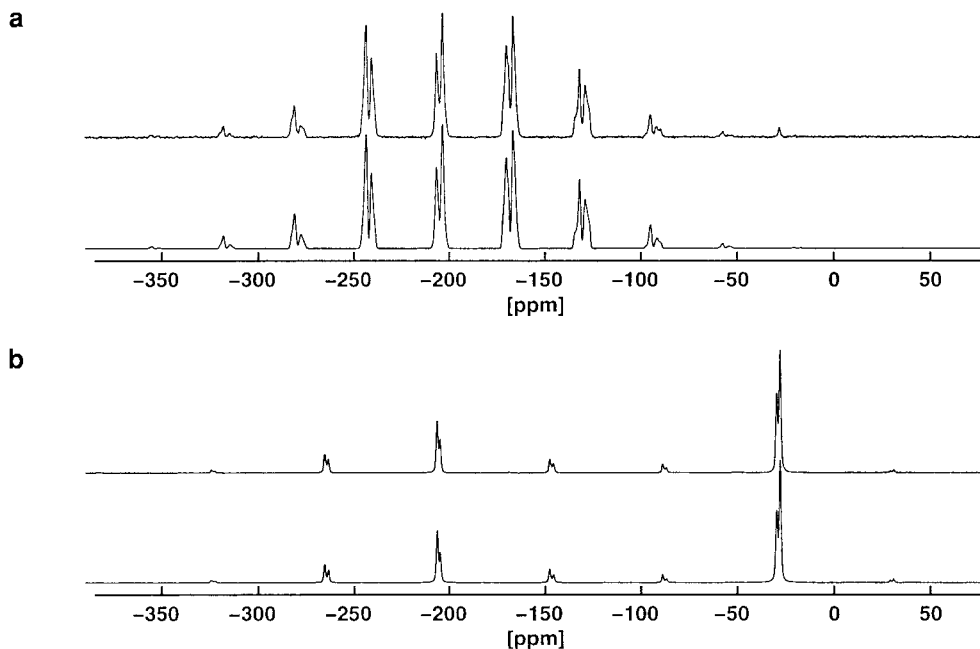For the determination of the relative orientations of the $^{13}C2$

FIG. 3. ^{13}C R^2 MAS NMR spectra ($\omega_0/2\pi = -100.6$ MHz) of two isotopomers of sodium pyruvate. The upper traces are experimental, and the lower traces are best-fit simulated spectra. (a) $n = 1$ ^{13}C R^2 MAS NMR spectra of **1-C1/C2;** $\omega_r/2\pi = 3739$ Hz; (b) $n = 3$ ^{13}C R^2 MAS NMR spectra of **1-C2/C3;** $\omega_r/2\pi = 5924$ Hz.

and ^{13}C3 CSA tensors, we switch to R^2 MAS NMR spectra of the ^{13}C two-spin system in **1-C2/C3** and to the corresponding CAS C_{23}, which is now defined by the PAS of the dipolar coupling tensor ω^{D23}. Given the large isotropic chemical shielding difference $\omega_{\rm iso}^{\Delta 23} = 176.8$ ppm for this spin pair and the small anisotropy of the ^{13}C3 chemical shielding tensor ($\delta^{\rm CS3} = 24$ ppm; see Table 1), $\beta_{\rm PC_{23}}^{\rm CS2}$ turns out to be the only orientational parameter which is sensitively encoded in the lineshapes of $n = 2, 3$ ^{13}C R^2 MAS NMR spectra of **1-C2/C3,** with minima for $\beta_{\rm PC_{23}}^{\rm CS2} \approx 90°$ and $\beta_{\rm PC_{23}}^{\rm CS2} \approx 270°$. As an example, experimental and simulated $n = 3$ ^{13}C R^2 MAS NMR spectra of **1-C2/C3** are shown in Fig. 3b. The small value $\delta^{\rm CS3} = 24$ ppm renders the determination of the orientation of the ^{13}C3 chemical shielding tensor from R^2 MAS NMR experiments impossible. For R^2 conditions with $1 \leq n \leq 6$, the ^{13}C3 orientational parameters are not sensitively encoded, while R^2 conditions with $n \geq 7$ would correspond to MAS frequencies so slow that heteronuclear dipolar coupling to nearby ^{23}Na spins-3/2 in the sodium pyruvate structure could no longer be neglected.

Even if only one orientational parameter, $\beta_{\rm PC_{23}}^{\rm CS2}$, can be extracted from ^{13}C R^2 MAS NMR spectra of **1-C2/C3,** we now have all the information necessary to derive the *absolute* orientation of the ^{13}C2 chemical shielding tensor. In both CAS, C_{12} and C_{23}, the angle $\beta_{\rm PC_{12}/PC_{23}}^{\rm CS2}$ is ca. 90° (or 270°). This means that the direction of the (most shielded) $\omega_{zz}^{\rm CS2}$ component of the ^{13}C2 CSA tensor is (nearly) perpendicular to the C1–C2 as well as to the C2–C3 bond direction. This is possible only if this direction is perpendicular to the C1–C2–C3 plane in the pyru-

vate moiety. With the y axis of CAS C_{12} defined as perpendicular to the C1–C2–C3 plane, it follows that $\gamma_{\rm PC_{12}}^{\rm CS2} = 90°$. Since $\alpha_{\rm PC_{12}}^{\rm CS2} = 10°$ has already been determined, now the *absolute* orientation of the ^{13}C2 CSA tensor in the molecular frame is known. The intermediate and the least shielded ^{13}C2 CSA tensor components are in the C1–C2–C3 plane, whereby the least shielded $\omega_{xx}^{\rm CS2}$ component is found to be collinear with the C1–C2 bond direction. Regarding the orientation of the ^{13}C1 CSA tensor, ^{13}C R^2 MAS NMR spectra of **1-C1/C2** yielded directly only the angle $\beta_{\rm PC_{12}}^{\rm CS1} \approx 0°$. This corresponds to the direction of the least shielded $\omega_{zz}^{\rm CS1}$ component of the ^{13}C1 CSA tensor being collinear with the C1–C2 bond direction as well as with the z axis of the ^{13}C1–^{13}C2 dipolar coupling tensor ω^{D12}. The angle $\alpha_{\rm PC_{12}}^{\rm CS1}$ describes a rotation around the z axis of the CSA tensor, and $\gamma_{\rm PC_{12}}^{\rm CS1}$ corresponds to a rotation around the z axis of the dipolar coupling tensor. With the directions of $\omega_{zz}^{\rm CS1}$ and ω_{zz}^{D12} coincident, the angles $\alpha_{\rm PC_{12}}^{\rm CS1}$ and $\gamma_{\rm PC_{12}}^{\rm CS1}$ describe identical rotations, and hence only rotations around ($\alpha_{\rm PC_{12}}^{\rm CS1} + \gamma_{\rm PC_{12}}^{\rm CS1}$) are relevant. Keeping this in mind, the multiple minima in the $\alpha_{\rm PC_{12}}^{\rm CS1}$–$\gamma_{\rm PC_{12}}^{\rm CS1}$ error plane depicted in Fig. 5 may now be resolved, as they are equivalent to the two minima found for an arbitrary value of, e.g., $\gamma_{\rm PC_{12}}^{\rm CS1} = 0°$. These two minima describe the following two indistinguishable orientations of the ^{13}C1 CSA tensor, where in both cases the least shielded $\omega_{zz}^{\rm CS1}$ component is oriented along the C1–C2 bond direction. With $\alpha_{\rm PC_{12}}^{\rm CS1} = 135°$ (alternatively, $\alpha_{\rm PC_{12}}^{\rm CS1} = 60°$) the most shielded $\omega_{xx}^{\rm CS1}$ component of the ^{13}C1 CSA tensor deviates by 29° (alternatively, $-46°$) from being perpendicular to the molecular COO plane. The direction of the most shielded $\omega_{xx}^{\rm CS1}$ component of
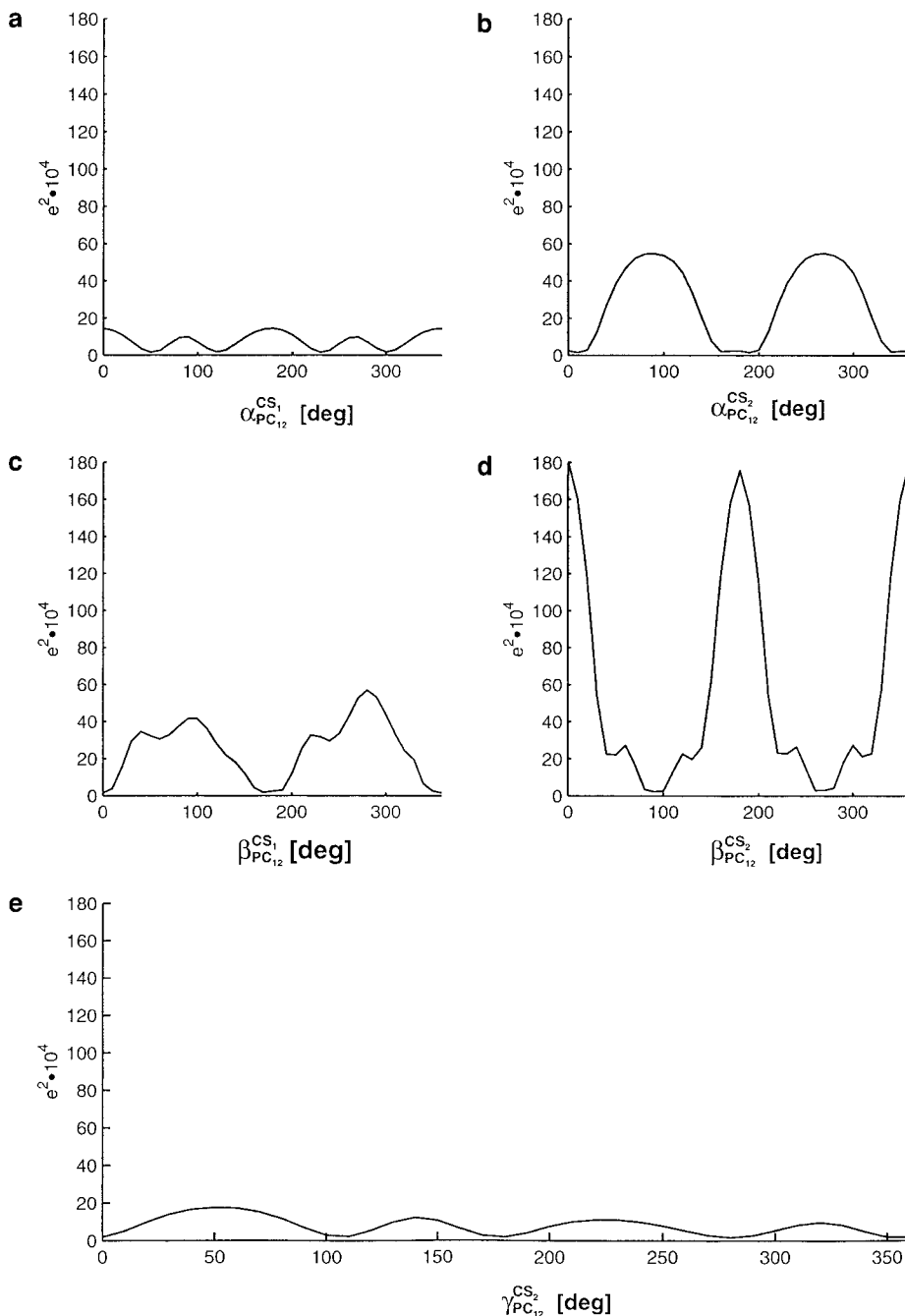
FIG. 4. Error scans for the individual fit parameters of the $n = 1$ ^{13}C R^2 MAS NMR spectrum of **1-C1/C2** depicted in Fig. 3a. $\gamma_{PC_{12}}^{CS_1} = 90°$ has been chosen arbitrarily; (a) $\alpha_{PC_{12}}^{CS_1}$, (b) $\alpha_{PC_{12}}^{CS_2}$, (c) $\beta_{PC_{12}}^{CS_1}$, (d) $\beta_{PC_{12}}^{CS_2}$, and (e) $\gamma_{PC_{12}}^{CS_2}$.

the ^{13}C1 CSA tensor precisely perpendicular to the COO plane would correspond to a value $\alpha_{PC_{12}}^{CS_1} = 106°$ as the C1–C2–C3 and COO planes in the pyruvate moiety are slightly twisted against each other.

An alternative route to the characterization of the ^{13}C chemical shielding tensors in the pyruvate moiety by means of ^{13}C R^2 MAS NMR would have been to use the ^{13}C three-spin system in **1-U^{13}C.** This option, however, would have had two

disadvantages. First, combining the information derived from separate experiments and calculations on the ^{13}C two-spin systems in **1-C1/C2** and **1-C2/C3** is computationally far more efficient than having to carry out rather time-consuming simulations and fitting procedures for a ^{13}C three-spin system. Second, mutual spatial isolation in the sodium pyruvate structure is better realized for the individual ^{13}C spin pairs in **1-C1/C2** and **1-C2/C3** than would have been the case for the
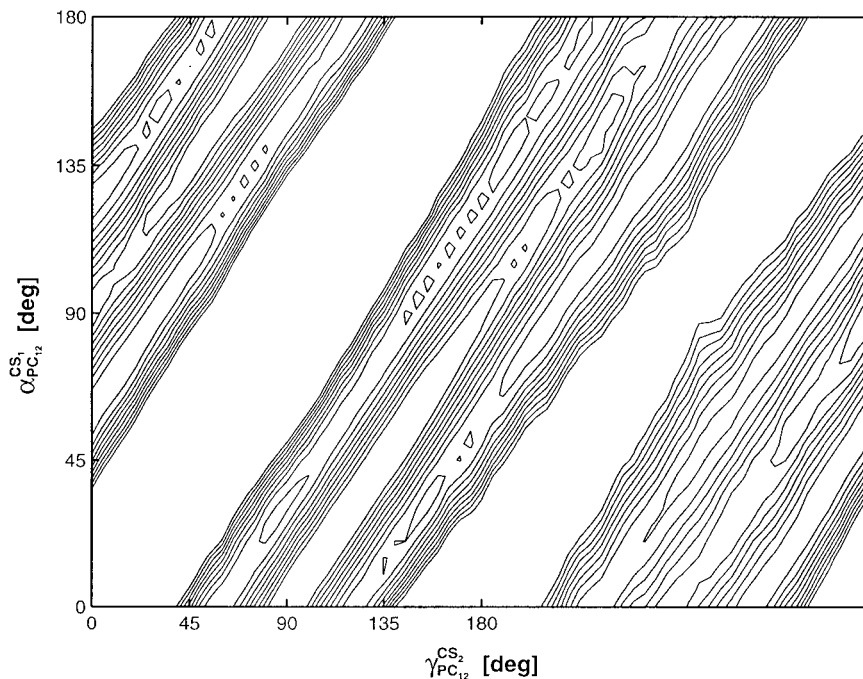
FIG. 5. Two-dimensional error map of fit parameters α_{PC12}^{CS1} and γ_{PC12}^{CS2} with $\gamma_{PC12}^{CS1} = 90°$ arbitrarily chosen. The contour lines are drawn at integer multiples N of the absolute minimum, $N = 1$–10; the calculation is based on an $n = 1$ ^{13}C R^2 MAS NMR spectrum of **1-C1/C2** with $\omega_0/2\pi = -125.8$ MHz and $\omega_r/2\pi = 4688$ Hz.

^{13}C three-spin system in **1-U^{13}C.** In any case, the properties of the pyruvate ^{13}C spin system are now sufficiently well known to serve next for the exploration of the performance of a recently proposed R^2-DQF scheme (*15*) in a more quantitative manner.

The R^2-DQF MAS NMR Experiment and Isolated Two-Spin Systems

As a general starting point, application of the R^2-DQF experiment (*15*) on a sample consisting of 90 wt% **1** and 10 wt% **1-C2/C3** is illustrated in Fig. 6. Figure 6a displays a conventional R^2 MAS NMR spectrum, with the $n = 1$ R^2 condition fulfilled for the ^{13}C2–^{13}C3 spin pair. The sharp ^{13}C resonances originating from **1** are clearly visible, as well as the R^2-broadened contributions from the **1-C2/C3** spin pair. The result of a R^2-DQF MAS NMR experiment on this sample, performed under otherwise identical conditions, is depicted in Fig. 6b: all non-spin-pair contributions are completely eliminated. With regard to the operational range of the R^2-DQF experiment (*15*) two points need to be considered in more detail. Point one concerns the dependence of the efficiency of the R^2-DQF experiment on the specific properties of a given homonuclear two-spin system. Point two concerns the spectral lineshapes passed through the R^2-DQF, and the question as to what extent the resulting lineshapes may be quantitatively analyzed by means of lineshape simulations.

The range of properties of a homonuclear spin pair which permit successful application of the R^2-DQF experiment is best characterized by numerical simulations. The results of numerical simulations are summarized in Figs. 7 and 8. Figure 7 illustrates how the relative magnitudes of ω_{iso}^{Δ} and b_{ij} in the absence of chemical shielding anisotropies (Figs. 7a, 7b) and of ω_{iso}^{Δ} and $\delta^{CS_{ij}}$ under the condition $b_{ij} \ll \omega_{iso}^{\Delta}$ (Figs. 7c–7e) are reflected in R^2-DQF lineshapes: whenever the magnitudes of b_{ij} or $\delta^{CS_{ij}}$ (or of both) are comparable to or exceed the magnitude of ω_{iso}^{Δ}, the resulting R^2-DQF spectra display spinning sidebands with phase distortions. With regard to the analysis of experimental R^2-DQF spectra of isolated two-spin systems by means of numerical simulations, the presence of spinning sidebands and/or phase distortions is not necessarily a problematic aspect. Of great importance for the practical applicability, however, is the dependence of the efficiency of the R^2-DQF experiment on the properties of a given spin system. This point is illustrated in Fig. 8 where R^2-DQF efficiencies are plotted as a function of τ_{exc} for different spin-system properties. The plots in Figs. 8a and 8b assume $b_{ij} < \omega_{iso}^{\Delta}$ as well as negligible chemical shielding anisotropies, $\delta^{CS_{ij}} = 0$, and otherwise represent two model situations typically arising for ^{13}C spin pairs in terms of homonuclear dipolar coupling constants b_{ij}. The model case with $b_{ij} = -300$ Hz describes a nondirectly bonded pair of carbon atoms at a distance of 294 pm from each other (Fig. 8a); the model case with $b_{ij} = -2000$ Hz mimics the situation of a pair of directly bonded carbon atoms (Fig. 8b). Both model situations yield essentially
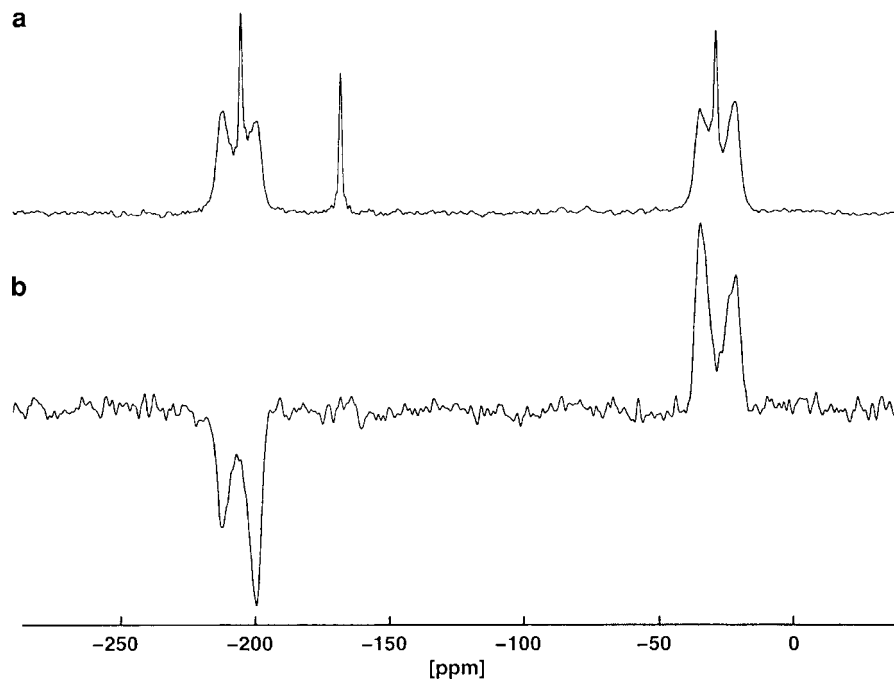
FIG. 6. ^{13}C MAS NMR spectra of a sample consisting of 90 wt% **1** and 10 wt% **1-C2/C3**, obtained at $\omega_0/2\pi = -50.3$ MHz and $\omega_r/2\pi = 8950$ Hz which fulfills the $n = 1$ R^2 condition for the ^{13}C2–^{13}C3 spin pair. (a) Conventional $n = 1$ R^2 MAS NMR spectrum; (b) R^2-DQF MAS NMR spectrum.

smooth "efficiency curves" and the efficiency of the R^2-DQF experiment is high for both large and small dipolar coupling constants b_{ij}. For $\delta^{CS_{ij}} = 0$ and realistic values of ω_{iso}^{Δ} the efficiency reaches the theoretical limit of ca. 73% for both b_{ij} model cases. This statement holds when $\omega_{iso}^{\Delta} > b_{ij}$, which is a fairly commonly occurring circumstance for ^{13}C spin systems in organic compounds. It is this range of spin-system properties (assumed in Figs. 8a, 8b) for which the theoretical explanations of the R^2-DQF experiment (*15*) apply. In the presence of nonnegligible chemical shielding anisotropies $\delta^{CS_{ij}}$ the efficiency of the R^2-DQF experiment depends in a highly complex manner on τ_{exc} as is depicted in Fig. 8c for a case with $\delta^{CS_{ij}} = 2\omega_{iso}^{\Delta}$. For instance, a difference in τ_{exc} of only 10 μs can make all the difference between a theoretical efficiency as low as 8% or as high as 22%. The strongly excitation-time-dependent efficiency shown in Fig. 8c is not a special property of the set of parameters chosen for this simulation. Similar calculations, employing different values $\delta^{CS_{ij}}$ and/or different sets of orientational parameters Ω_{PC}^{CS}, show similarly strong and fast oscillations of the R^2-DQF efficiency as a function of τ_{exc}. In summary, the numerical simulations define that $\delta^{CS_{ij}}$ must not exceed ω_{iso}^{Δ}, or preferably be considerably less than ω_{iso}^{Δ}, in order for the R^2-DQF experiment to yield high efficiency in a straightforward manner. For this regime it is also possible to reasonably predefine τ_{exc} for optimum excitation based on b_{ij} considerations alone. The numerical simulations imply that *in principle* also for cases where the $\delta^{CS_{ij}}$ amount to a nonnegligible fraction of ω_{iso}^{Δ} fairly high R^2-DQF efficiencies are possible. In practice, however, experimentally finding the R^2-DQF

conditions for which this is the case may require extensive experimental search operations. There are no obvious or clear-cut criteria for how to predict or preselect such narrow optimum conditions arising from the complicated interplay of τ_{exc}, ω_{iso}^{Δ}, b_{ij}, $\delta^{CS_{ij}}$, and Ω_{PC}^{CS}. The numerical simulations so far essentially deal with ideal spin-pair circumstances, equivalent to the assumption of, e.g., perfect ^{1}H decoupling performance, and hence only give an impression of the best possible performance of the pulse sequence, depending on the inherent properties of a spin pair in the absence of any experimental shortcomings. How these expectations are met in practice is a different question and will be considered next.

Applied to the ^{13}C spin system in the pyruvate moiety, numerical simulations suggest that the ^{13}C1–^{13}C2 spin pair in **1-C1/C2** is a less suitable target for experimental R^2-DQF MAS NMR explorations because the $\delta^{CS_{1,2}}$ exceed $\omega_{iso}^{\Delta_{12}}$. The ^{13}C2–^{13}C3 spin pair in **1-C2/C3**, however, features more convenient properties regarding the efficiency of the R^2-DQF experiment ($b_{23} = -2259$ Hz, $\delta^{CS_2} = 0.62 \, \omega_{iso}^{\Delta_{23}}$, $\delta^{CS_3} = 0.14 \, \omega_{iso}^{\Delta_{23}}$). In order to evaluate which parameters may be extracted from experimental R^2-DQF lineshapes, it is first necessary to ensure that the numerical simulations precisely reproduce the experimental data. To check this, we take advantage of the known parameters (*vide supra*) of the ^{13}C2–^{13}C3 spin pair in **1-C2/C3**. Figures 9b–9f compare experimental and simulated R^2-DQF lineshapes for this ^{13}C spin pair for a range of different excitation periods $\tau_{exc} = 100 \, \mu$s to $\tau_{exc} = 500 \, \mu$s. Obviously, the numerical simulations reproduce very well the experimentally observed lineshapes as a function of τ_{exc}, including phases
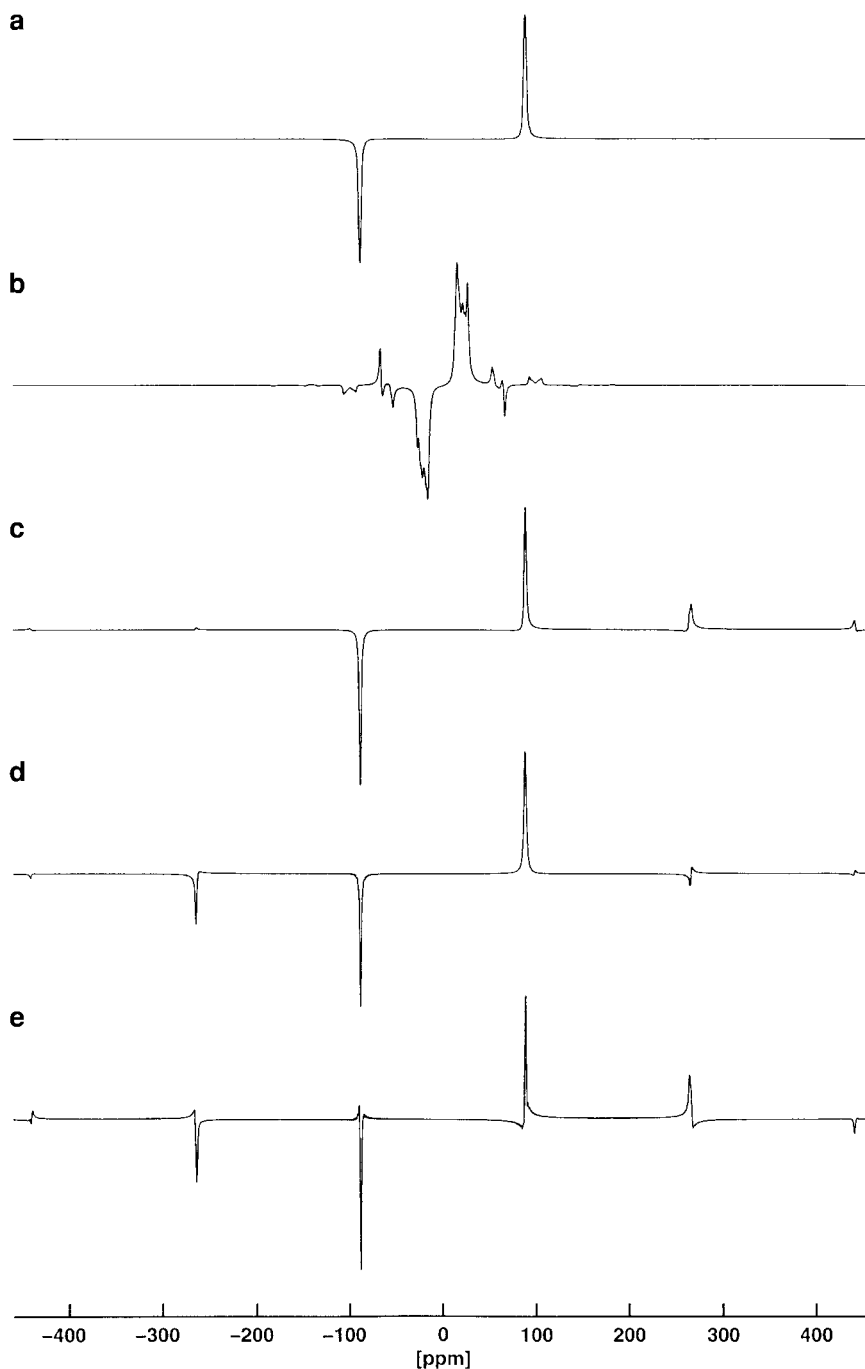
FIG. 7. Simulated R^2-DQF lineshapes for an isolated two-spin system (S_i, S_j) with positive gyromagnetic ratio and assuming the following parameters. (a) $b_{ij} = -300$ Hz, $\delta^{CSij} = 0$, $\omega_{iso}^{\Delta ij} = 8887$ Hz, $\tau_{exc} = 3.3$ ms; (b) $b_{ij} = -2000$ Hz, $\delta^{CSij} = 0$, $\omega_{iso}^{\Delta ij} = 2000$ Hz, $\tau_{exc} = 220$ μs; (c) $b_{ij} = -300$ Hz, $\delta^{CSi} = 0$, $\delta^{CSj} = 2\omega_{iso}^{\Delta ij}$, $\tau_{exc} = 3.3$ ms; (d) $b_{ij} = -300$ Hz, $\delta^{CSi} = 2\omega_{iso}^{\Delta ij}$, $\delta^{CSj} = 0$, $\tau_{exc} = 3.3$ ms; (e) $b_{ij} = -300$ Hz, $\delta^{CSi} = \delta^{CSj} = 2\omega_{iso}^{\Delta ij}$, $\tau_{exc} = 3.3$ ms. The simulations in (c)–(e) employ arbitrarily chosen sets of Euler angles $\Omega_{PC}^{CSi} = \{10, 0, 90\}$, $\Omega_{PC}^{CSj} = \{90, 0, 0\}$, and $\eta^{CSij} = 0$.

and phase distortions. There are distinct differences between conventional R^2 and R^2-DQF lineshapes, experimentally as well as numerically (compare Fig. 9a to Figs. 9b–9f). Numerical simulation predicts a maximum possible R^2-DQF efficiency of 47% for the $^{13}C2$–$^{13}C3$ spin pair in **1-C2/C3** to occur at a duration of the excitation period $\tau_{exc} = 320$ μs. Experi-

mentally we find a maximum efficiency of 35% for the predicted value of τ_{exc} (see Fig. 10). An efficiency of 35% would require roughly eight times the amount of spectrometer time to achieve the same signal-to-noise ratio in a R^2-DQF MAS NMR spectrum as would be obtained in the corresponding conventional R^2 MAS NMR spectrum. The differences between cal-
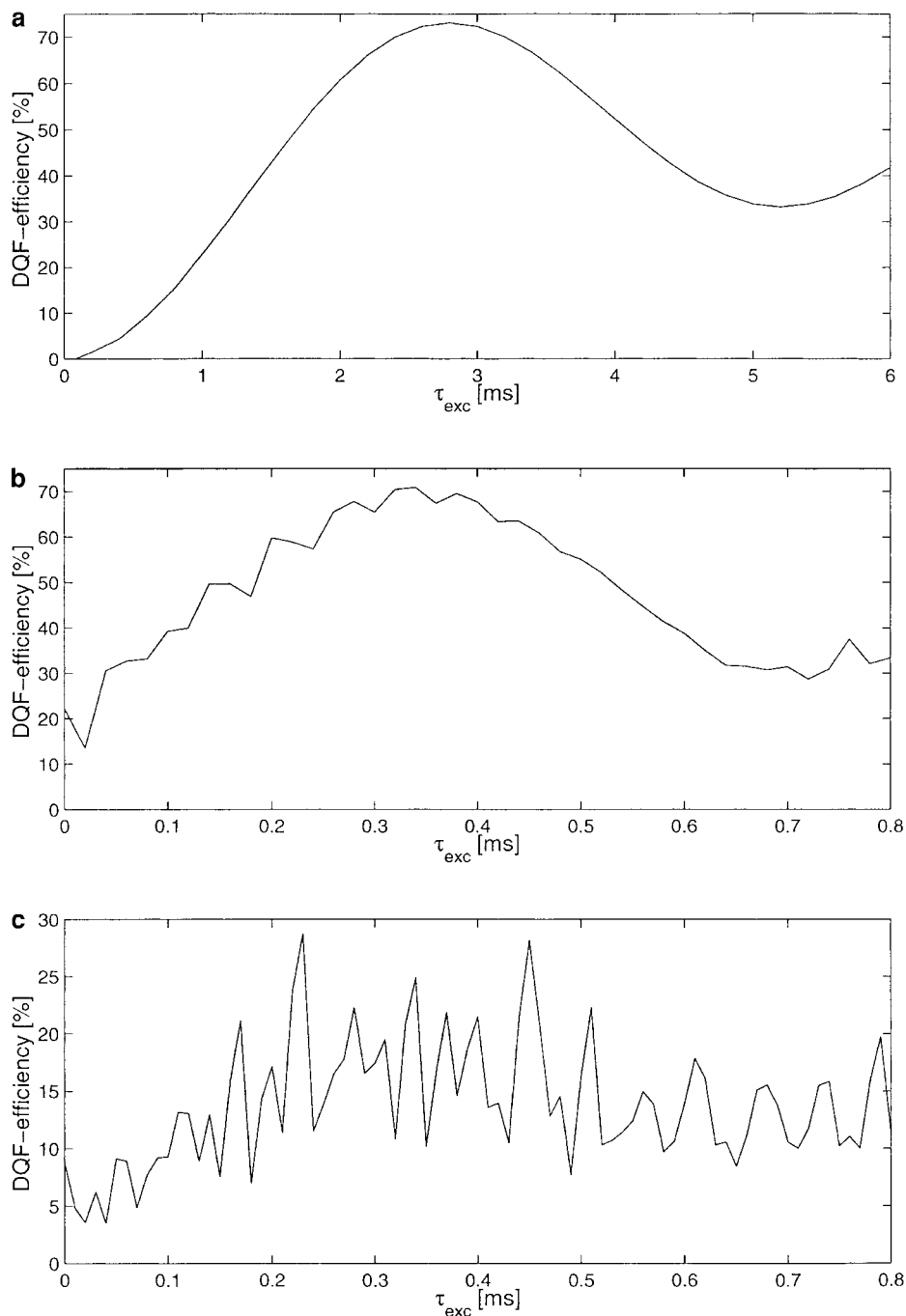
FIG. 8. Theoretical R^2-DQF efficiencies plotted as a function of τ_{exc}, for an isolated two-spin system (S_i, S_j) with positive gyromagnetic ratio, $\omega_{iso}^{\Delta ij} = 8887$ Hz, and assuming the following parameters. (a) $b_{ij} = -300$ Hz, $\delta^{CS ij} = 0$; (b) $b_{ij} = -2000$ Hz, $\delta^{CS ij} = 0$; (c) $b_{ij} = -2000$ Hz, $\delta^{CS i} = \delta^{CS j} = 2\omega_{iso}^{\Delta ij}$, $\eta^{CS ij} = 0$, $\Omega_{PC}^{CS i} = \{10, 0, 90\}$, and $\Omega_{PC}^{CS j} = \{90, 0, 0\}$.

culated and experimentally observed R^2-DQF efficiencies (see Fig. 10) slightly increase for increasing values of τ_{exc}. This finding may be ascribed to the negative side effects of less than perfect ^{1}H decoupling performance, a ubiquitous topic of concern for all kinds of experimental MAS NMR circumstances, regardless of the zero-, single-, or double-quantum nature of the pulse sequence applied.

Next, we consider which of the parameters describing the ^{13}C2–^{13}C3 spin pair are sensitively encoded in the R^2-DQF lineshapes of **1-C2/C3** and how these various sensitivities compare to the conventional $n = 1$ R^2 MAS NMR situation. For the ^{13}C2–^{13}C3 spin pair, the only parameter sensitively encoded in $n = 1$ R^2 MAS NMR spectra is b_{23}. A similar picture emerges for the R^2-DQF lineshapes of the ^{13}C2–^{13}C3
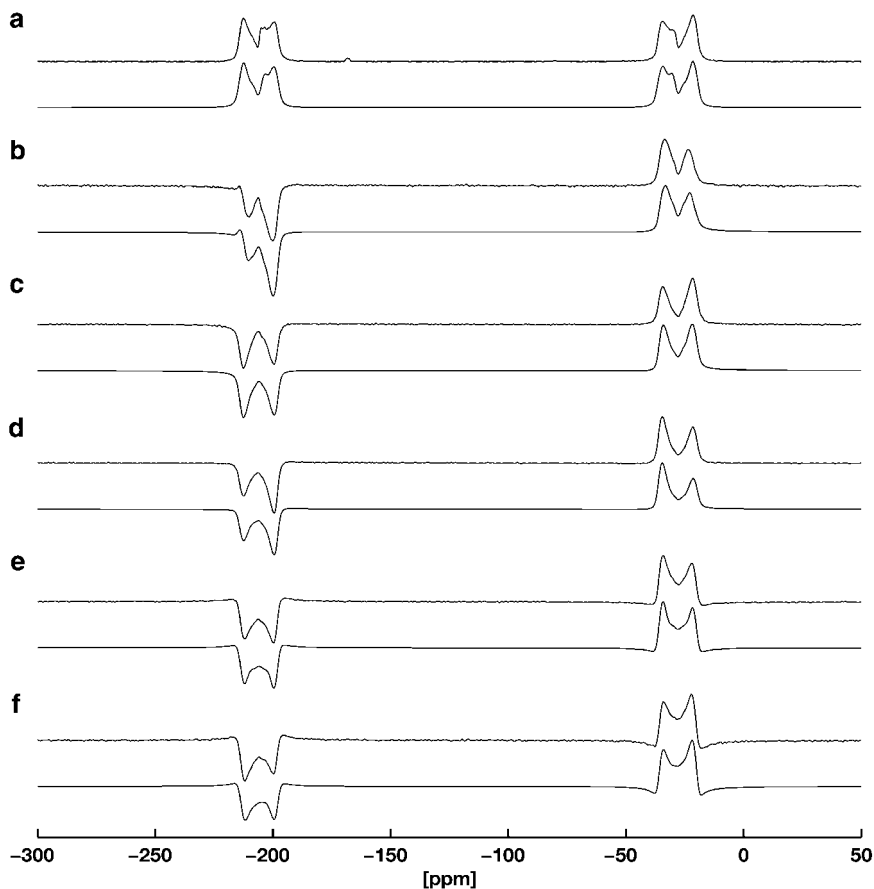
FIG. 9. (a) Experimental (upper trace) and simulated (lower trace) conventional $n = 1$ ^{13}C R^2 lineshapes of **1-C2/C3** at $\omega_0/2\pi = -50.3$ MHz and $\omega_r/2\pi = 8950$ Hz. (b–f) Experimental (upper traces) and simulated (lower traces) ^{13}C R^2-DQF lineshapes of **1-C2/C3** at $\omega_0/2\pi = -50.3$ MHz and $\omega_r/2\pi = 8950$ Hz for different values of τ_{exc}: $\tau_{exc} = 500$ μs (b), $\tau_{exc} = 400$ μs (c), $\tau_{exc} = 300$ μs (d), $\tau_{exc} = 200$ μs (e), and $\tau_{exc} = 100$ μs (f).

spin pair. One-dimensional error scans for all ^{13}C2–^{13}C3 spin-pair parameters reveal that under the $n = 1$ R^2 condition b_{23} is by far the most sensitive fit parameter, with similar sensitivities for the R^2 and R^2-DQF experiments (see Fig. 11). For both experiments a well-defined, sharp minimum for b_{23} is found at the value corresponding to the internuclear C2–C3 distance in sodium pyruvate predicted by X-ray diffraction. The second most sensitive fit parameter, again for both the $n = 1$ R^2 and the R^2-DQF experiment, is $\beta_{PC_{23}}^{CS_2}$. For this parameter, however, the sensitivity in both experiments is more than an order of magnitude less than that for b_{23}. This finding for the ^{13}C2–^{13}C3 spin pair in **1-C2/C3** should not be misread in the sense that it might be generally "safe" to ignore magnitudes and orientations of chemical shielding tensors when aiming solely at the estimation of internuclear distances from R^2 or R^2-DQF MAS NMR experiments. That b_{23} turns out to be the only sensitively encoded parameter for the ^{13}C2–^{13}C3 spin pair is a specific property of this particular spin pair. The R^2 vs R^2-DQF line-shape-sensitivity comparison rather suggests something different. It indicates that those parameters which happen to be sensitively encoded in conventional $n = 1$ R^2 lineshapes of a given spin pair can also be retrieved by numerical simulations

from R^2-DQF lineshapes, provided that a sufficiently good signal-to-noise ratio is achieved in the experimental R^2-DQF spectra. Which parameters then may or may not be sensitive lineshape-fit parameters is governed by the properties of the spin system, for the R^2 as well as the R^2-DQF MAS NMR experiment.

The experiments on the ^{13}C spin pair in **1-C2/C3** in conjunction with numerical simulations so far have illustrated trends and general properties of the R^2-DQF experiment (*15*) and have indicated which parameters may be extracted from the resulting R^2-DQF lineshapes of isolated spin pairs. However, to some extent isolated two-spin systems such as the ^{13}C spin pair in **1-C2/C3** represent an artificial model situation. With regard to realistic application situations it is also important to learn about the performance of the R^2-DQF experiment if the condition of an isolated spin pair in the sample no longer holds.

The R^2-DQF MAS NMR Experiment and Multiple-Spin Systems

One step up in the complexity of the spin-system properties is present in the ^{13}C three-spin system in **1-U^{13}C** under various

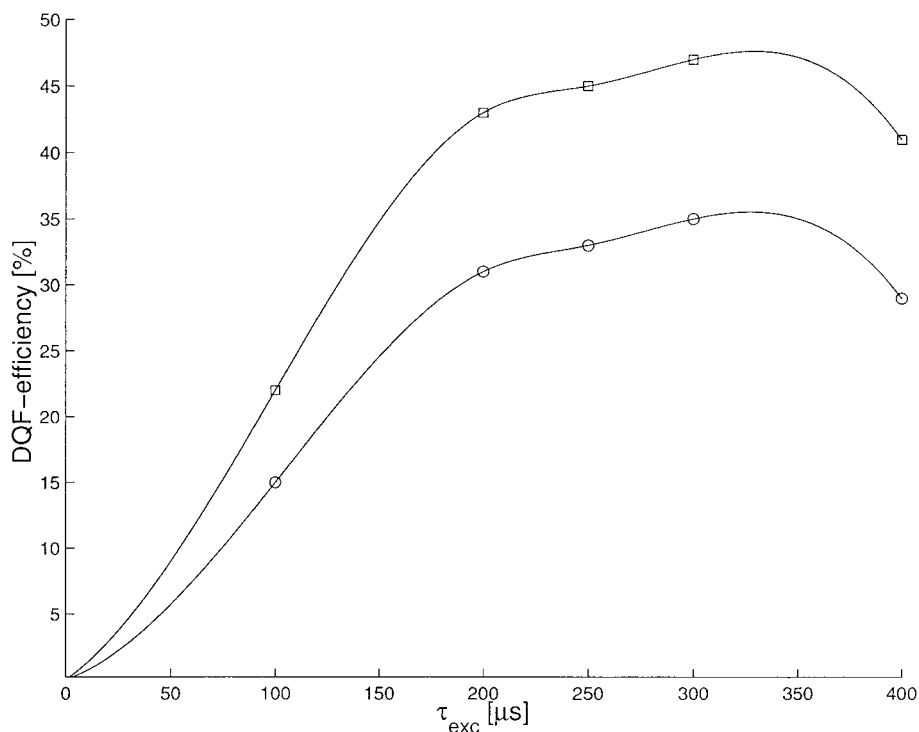**FIG. 10.** Theoretical ($\square$) and experimental ($\bigcirc$) R^2-DQF efficiencies for the ^{13}C2–^{13}C3 spin pair in **1-C2/C3** at $\omega_0/2\pi = -50.3$ MHz, $\omega_r/2\pi = 8950$ Hz, and values of τ_{exc} ranging from 100 to 500 μs (compare Figs. 9b–9f).
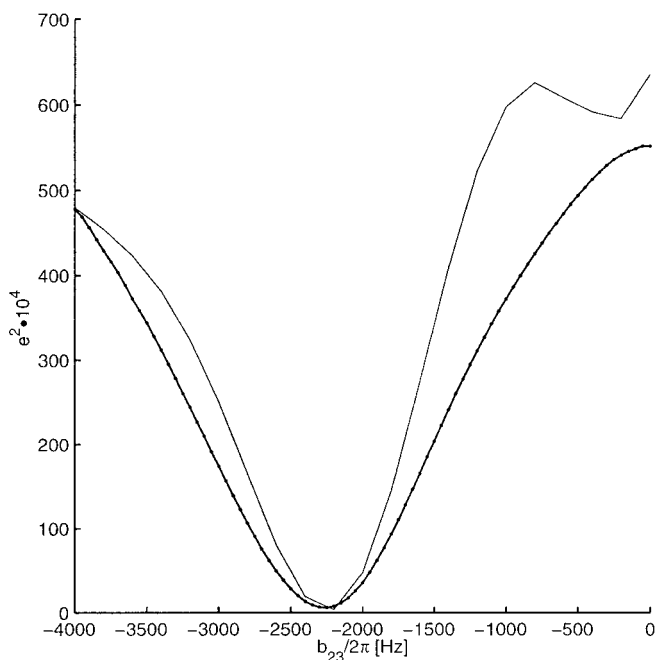

FIG. 11. Comparison of sensitivity of lineshape-fit parameter b_{23} for the conventional $n = 1$ R^2 condition ($\bullet\bullet\bullet$) and the corresponding R^2-DQF experiment (—), based on experimental spectra of the ^{13}C2–^{13}C3 spin pair in **1-C2/C3** at $\omega_0/2\pi = -50.3$ MHz and $\omega_r/2\pi = 8950$ Hz.

R^2-DQF conditions. With the experimental R^2-DQF conditions adjusted for selection of the ^{13}C2–^{13}C3 spin pair, the ^{13}C1 resonance of **1-U^{13}C** is nearly completely absent in the resulting experimental R^2-DQF NMR spectrum (see Fig. 12b). Moreover, the R^2-DQF lineshape for the ^{13}C2–^{13}C3 spin pair in **1-U^{13}C** is not significantly different from the R^2-DQF lineshape previously observed for the selectively pairwise ^{13}C-labeled sample **1-C2/C3** under otherwise identical conditions (compare Fig. 9b). Accordingly, two-spin simulations for the ^{13}C2–^{13}C3 spin pair would have yielded the correct C2–C3 distance, in spite of using the ^{13}C three-spin system in **1-U^{13}C** and ignoring the presence of the third, ^{13}C1, spin. This kind of pseudo-spin-pair behavior in a three-spin system is not a property of the R^2-DQF experiment but rather a property of a particular given spin system and occasionally occurs also under conventional R^2 MAS NMR conditions (*31*). Adjusting the experimental R^2-DQF conditions precisely as required for the selection of the ^{13}C1–^{13}C3 spin pair in **1-U^{13}C** according to the known parameters of this spin pair yields the spectrum depicted in Fig. 12c, to which in addition to the two selected ^{13}C1, ^{13}C3 resonances a considerable fraction of the ^{13}C2 resonance contributes. Slight misadjustments/"detuning" of the experimental parameters (excitation period, offset and MAS frequencies) from the predicted optimum selection conditions helps to
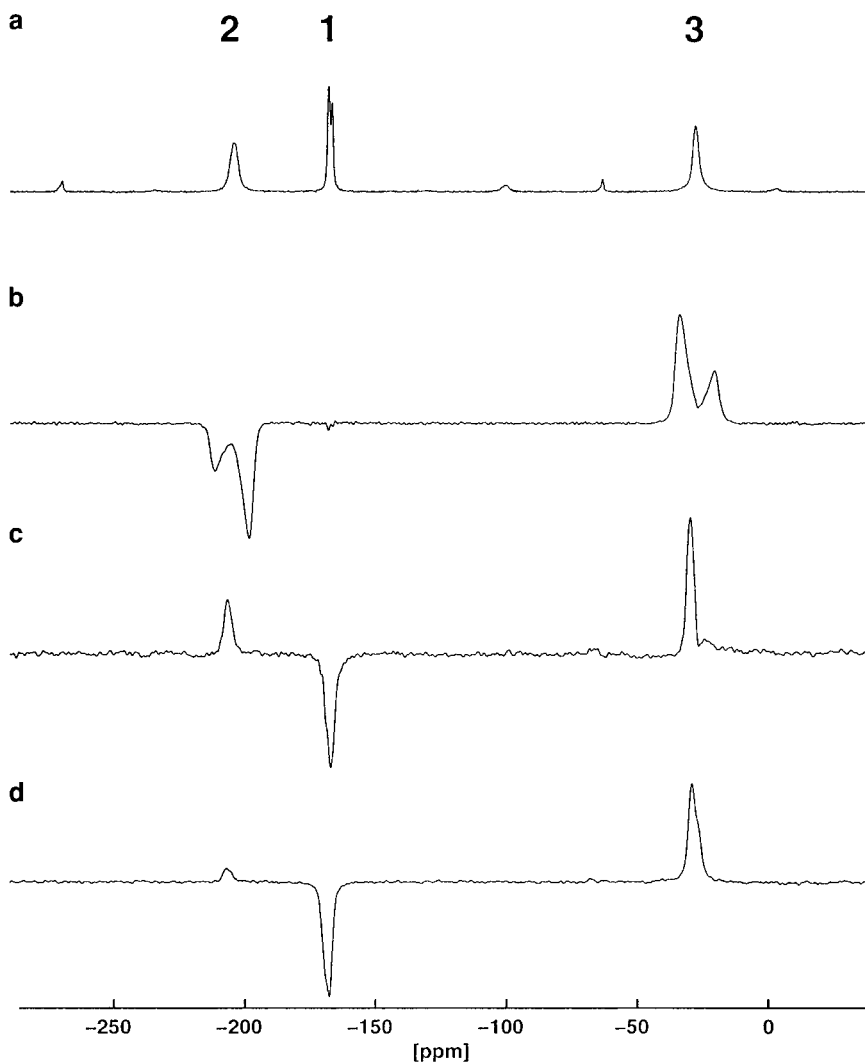
FIG. 12. Experimental ^{13}C MAS NMR spectra of **1-U^{13}C** ($\omega_0/2\pi = -50.3$ MHz). (a) Off-R^2 MAS NMR spectrum, $\omega_r/2\pi = 5198$ Hz; (b) R^2-DQF spectrum with parameters adjusted for selection of the ^{13}C2–^{13}C3 pair ($\omega_r/2\pi = 8950$ Hz, $\tau_{exc} = 300$ μs); (c and d) R^2-DQF spectra with parameters adjusted for selection of the ^{13}C1–^{13}C3 pair ($\tau_{exc} = 2$ ms) with slightly different MAS frequencies $\omega_r/2\pi = 7020$ Hz (c) and $\omega_r/2\pi = 7070$ Hz (d). The selectivity of the R^2-DQF performance for the ^{13}C2–^{13}C3 spin pair in **1-U^{13}C** is found to be less sensitive to variation of the experimental parameters.

improve the filtration selectivity for the ^{13}C1–^{13}C3 spin pair in **1-U^{13}C** (see Fig. 12d). The fairly uncharacteristic, minor broadening of the R^2-DQF lineshapes of the ^{13}C1, ^{13}C3 resonances obviously does not provide a suitable starting condition for an estimation of, e.g., the C1–C3 distance based on lineshape simulations, regardless of the need to carry out two- or three-spin simulations. Qualitatively the experimental R^2-DQF results on **1-U^{13}C** indicate that, in terms of filtration selectivity, the R^2-DQF MAS NMR experiment may be successfully employed for spin systems with more than two spins.

In order to investigate this question a little further, we switch to a sample containing a true multiple-^{13}C-spin system. The structure of L-tyrosine-ethylester (*17*) shows that the molecular units are spatially not well separated from each other; the 11 ^{13}C spins per molecule in **2-U^{13}C** (see Fig. 1) accordingly do

not even represent an isolated 11-spin system. In addition, it is known that at ambient conditions in solid L-tyrosine-ethylester the phenyl ring undergoes π flips around the C1–C4 axis with a rate constant of 90 Hz at $T = 295$ K (*32*). The assignment of the 11 ^{13}C resonances of **2-U^{13}C** is indicated in Fig. 13 in a ^{13}C CP MAS NMR spectrum of **2** (obtained at $T = 250$ K); the numbering scheme C1 to C11 follows the numbering scheme used in the crystal structure determination (*17*). Several different pairs of ^{13}C spins in **2-U^{13}C** are not afflicted by the π flips of the phenyl ring and should, in principle, have properties suitable for application of the R^2-DQF experiment.

In the L-tyrosine-ethylester molecule the ethyl group is bent backward over the phenyl ring ("scorpion-like") which leads to a relatively short intramolecular distance of 504 pm between ^{13}C1 and ^{13}C10. The corresponding dipolar coupling constant
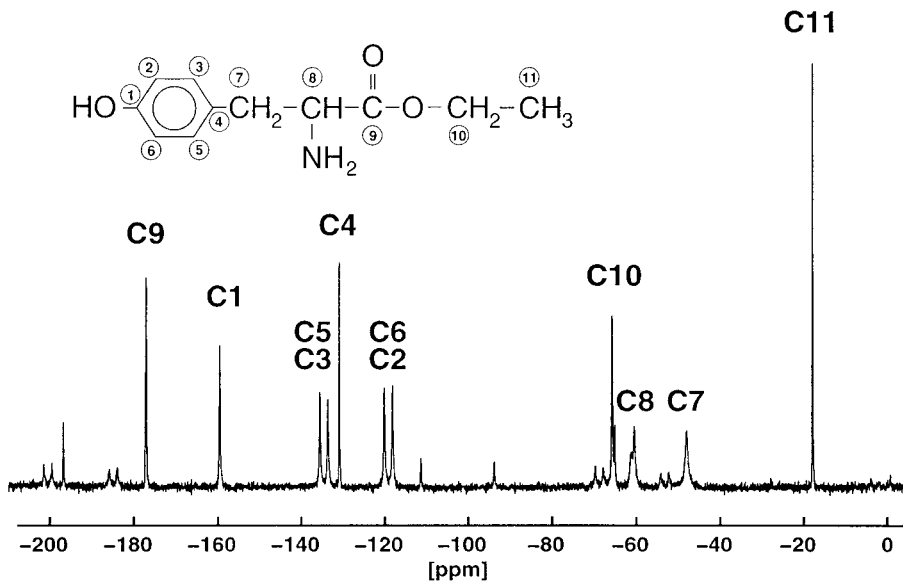
FIG. 13. ^{13}C CP MAS NMR spectrum of **2** at $T = 250$ K, $\omega_0/2\pi = -75.5$ MHz, and $\omega_r/2\pi = 4970$ Hz. The assignment of the ^{13}C resonances (*32*) is indicated.

of only -59 Hz necessitates long excitation periods $\tau_{exc} \approx 5$ ms for optimum selection of the ^{13}C1–^{13}C10 spin pair. This requirement prevents successful R^2-DQF selection of the ^{13}C1–^{13}C10 resonances in **2-U^{13}C** (see Fig. 14b). The ^{13}C1–^{13}C10 spin pair in selectively pairwise ^{13}C1, ^{13}C10-enriched L-tyrosine-ethylester is a "classical target" for the evaluation of R^2 MAS NMR techniques (*33, 34*); even for selectively ^{13}C1, ^{13}C10-enriched L-tyrosine-ethylester accurate determination of this internuclear distance requires application of improved R^2 MAS NMR techniques such as R^2 tickling experiments (*34*). R^2-DQF matters improve when adjusting the experimental conditions for selection of the ^{13}C9–^{13}C10 pair in **2-U^{13}C**, as can be seen in Fig. 14c. Here the isotropic chemical shielding difference is slightly larger than that for the ^{13}C1–^{13}C10 pair, the optimum offset region is slightly less "central" in the spectral region, and, more importantly, the ^{13}C9–^{13}C10 internuclear distance of 238 pm allows for shorter excitation periods $\tau_{exc} \approx 1$ ms. Experimental R^2-DQF MAS NMR spectra of **2-U^{13}C,** optimized for selection of the ^{13}C9–^{13}C10 pair, show less contamination by unwanted additional ^{13}C resonances for a range of experimental conditions. Closer inspection, however, reveals that not only the ^{13}C9–^{13}C10 pair but also the ^{13}C8–^{13}C9 pair contributes to this R^2-DQF lineshape. Simulated R^2-DQF spectra assuming an isolated ^{13}C9–^{13}C10 spin pair do not match the experimentally observed lineshapes, with the latter pointing toward a larger effective dipolar coupling constant than is predicted by the ^{13}C9–^{13}C10 internuclear distance. The structure of L-tyrosine-ethylester convincingly explains these discrepancies. ^{13}C9 is directly bonded to ^{13}C8, and the ^{13}C8 resonance is only 5.0 ppm away from the ^{13}C10 resonance. In addition, the carbonyl group is the part of the molecule where the closest spatial contacts with the ester

functionality of neighboring molecules in the structure occur. In consequence, contributions from at least the three ^{13}C9, ^{13}C10, ^{13}C8 spins within the molecule contribute to the ^{13}C9–^{13}C10 selection-optimized R^2-DQF lineshape of **2-U^{13}C.**

Finally, the ^{13}C10–^{13}C11 pair in **2-U^{13}C** appears as a nearly ideally suited target for the R^2-DQF experiment. The ethyl group forms a relatively isolated subunit in the L-tyrosine-ethylester molecule. The combination of very small δ^{CS} for both ^{13}C spins, a short internuclear distance (139 pm) allowing for short optimum excitation periods $\tau_{exc} \approx 300$ μs, and an optimum offset frequency well away from the central spectral region leads us to expect robust R^2-DQF performance for this pair of resonances in **2-U^{13}C.** At a ^{13}C Larmor frequency $\omega_0/2\pi = -50.3$ MHz the difference in isotropic chemical shielding for the ^{13}C10, ^{13}C11 resonances (47.8 ppm) corresponds to an $n = 1$ R^2 condition of $\omega_r/2\pi = 2404$ Hz, less than the dipolar coupling constant (-2858 Hz) for this spin pair. The expected R^2-DQF lineshape for the ^{13}C10–^{13}C11 pair at $\omega_0/2\pi = -50.3$ MHz, based on two-spin simulations employing the known dipolar coupling constant and neglecting chemical shielding anisotropies, is depicted in Fig. 15a. Note the presence of sidebands and pronounced phase distortions, both of dipolar coupling origin. Experimental R^2-DQF spectra of **2-U^{13}C,** optimized for selection of the ^{13}C10–^{13}C11 pair, display lineshapes very different from those of the simulated spectrum: there are hardly any phase distortions or sidebands (see Fig. 15b). The spectral contribution of the ^{13}C10–^{13}C11 pair is selectively passed through the R^2-DQF for quite a range of excitation times and offset and MAS frequencies. The only possibility of reproducing numerically the experimentally observed R^2-DQF lineshapes for the ^{13}C10–^{13}C11 pair is to

FIG. 14. Experimental ^{13}C MAS NMR spectra of **2-U^{13}C** ($\omega_0/2\pi = -50.3$ MHz) at room temperature. (a) Off-R^2 MAS NMR spectrum, $\omega_r/2\pi = 7040$ Hz. (b) R^2-DQF spectra with parameters adjusted for selection of the ^{13}C1–^{13}C10 pair with $\omega_r/2\pi = 4730$ Hz; top: $\tau_{exc} = 5.0$ ms; bottom: $\tau_{exc} = 3.0$ ms; no combination of experimental parameters $\omega_r/2\pi$, τ_{exc}, and offset frequency for successful selection of the ^{13}C1–^{13}C10 pair could be found. (c) R^2-DQF spectra with parameters adjusted for selection of the ^{13}C9–^{13}C10 pair with $\omega_r/2\pi = 5574$ Hz; top: $\tau_{exc} = 1.5$ ms; bottom: $\tau_{exc} = 0.5$ ms; note that the latter spectrum appears more selective, but essentially is dominated by contributions from the ^{13}C8–^{13}C9 pair rather than by the intended ^{13}C9–^{13}C10 selection.
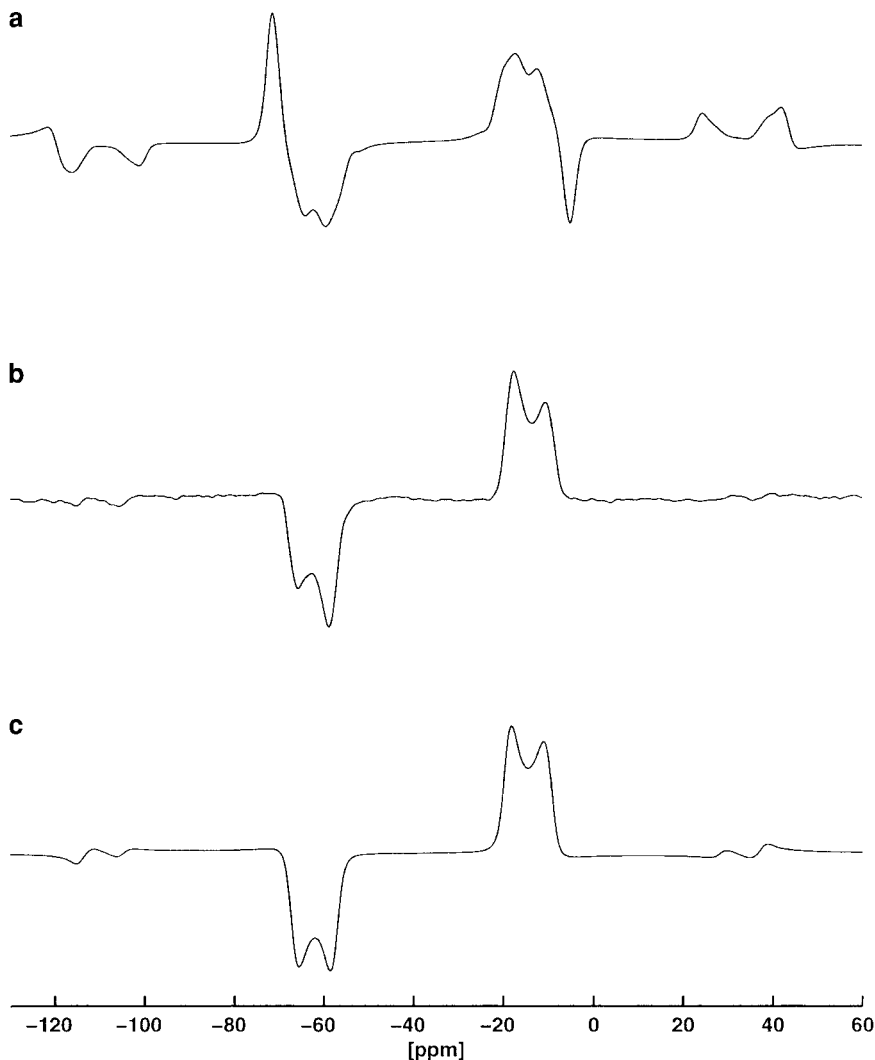
FIG. 15. ^{13}C R^2-DQF spectra of **2-U^{13}C** ($\omega_0/2\pi = -50.3$ MHz, $\omega_r/2\pi = 2404$ Hz, $\tau_{exc} = 200$ μs) at room temperature, focused on selection of the ^{13}C10–^{13}C11 pair. (a) Simulated R^2-DQF spectrum, assuming an isolated ^{13}C10–^{13}C11 spin pair, neglecting chemical shielding anisotropies, and employing a dipolar coupling constant of -2858 Hz, corresponding to the internuclear ^{13}C10–^{13}C11 distance determined by X-ray diffraction (*17*). (b) Experimental R^2-DQF spectrum. (c) Simulated R^2-DQF spectrum of the ^{13}C10–^{13}C11 pair, assuming an effective dipolar coupling constant of -1400 Hz.

assume a strongly reduced effective dipolar coupling constant (-1400 Hz instead of -2858 Hz as calculated from the structure; see Fig. 15c). This, in turn, can be explained by the presence of yet another dynamic process, in addition to the π flips of the phenyl ring, engaging the ethyl group in solid L-tyrosine-ethylester and leading to partial averaging of the dipolar coupling interaction within the ^{13}C10–^{13}C11 pair. Indications of dynamic disorder of the ethyl group are also found in X-ray diffraction experiments (*17*), and are observed in simulations of conventional R^2 MAS NMR spectra of this spin pair, as well as in 2D ^{13}C RIL (*35, 36*) MAS NMR experiments on **2-U^{13}C**, where even at $T = 240$ K we find spin-diffusion build-up rate constants between ^{13}C10 and ^{13}C11 which are systematically less than is expected from the known X-ray diffraction structure (*32*).

SUMMARY

In conclusion, we briefly summarize the most important implications of the features of the recently proposed R^2-DQF (*15*) experiment, based on our numerical and experimental results described above.

1. Numerical simulations predict robust and smooth R^2-DQF performance with high efficiency for large *and* small dipolar coupling interactions in the absence of chemical shielding anisotropies.

2. In the presence of nonnegligible chemical shielding anisotropies the R^2-DQF efficiencies vary strongly and in a complex manner with τ_{exc}: the pronounced variations of the efficiencies reflect the interplay of τ_{exc}, ω_{iso}^{Δ}, b_{ij}, $\delta^{CS_{ij}}$, and Ω_{PC}^{CS}.

3. Numerical simulations in conjunction with experiments demonstrate that for isolated spin systems (i) experimental R^2-DQF lineshapes may be reproduced numerically with high precision, and (ii) those spin-system parameters which are sensitively encoded in the corresponding conventional $n = 1$ R^2 lineshapes can be quantitatively retrieved also from R^2-DQF lineshapes.

4. Experiments in conjunction with some numerical simulations on multiple-^{13}C-spin systems indicate possibilities and limitations for the application of the R^2-DQF experiment on nonisolated spin systems: for certain favorable spin-system properties the experiment holds promise for solving structure determination tasks on spin systems with more than two spins. In particular the option to detect and possibly quantify localized molecular dynamic properties in multiple-^{13}C-spin systems may turn out to be an important feature, adding "safety" and precision to solid-state NMR structural investigations on multiply or fully ^{13}C-enriched organic solids.

ACKNOWLEDGMENTS

REFERENCES

1. E. R. Andrew, A. Bradbury, R. G. Eades, and V. T. Wynn, Nuclear cross relaxation induced by specimen rotation, *Phys. Lett.* **4,** 99–100 (1963).

2. D. P. Raleigh, M. H. Levitt, and R. G. Griffin, Rotational resonance in solid state NMR, *Chem. Phys. Lett.* **146,** 71–76 (1988).

3. M. H. Levitt, D. P. Raleigh, F. Creuzet, and R. G. Griffin, Theory and simulations of homonuclear spin pairs in rotating solids, *J. Chem. Phys.* **92,** 6347–6364 (1990).

4. A. Kubo and C. A. McDowell, One- and two-dimensional ^{31}P cross-polarization magic-angle-spinning nuclear magnetic resonance studies on two-spin systems with homonuclear dipolar and J coupling, *J. Chem. Phys.* **92,** 7156–7170 (1990).

5. A. Schmidt and S. Vega, The Floquet theory of nuclear magnetic resonance spectroscopy of single spins and dipolar coupled spin pairs in rotating solids, *J. Chem. Phys.* **96,** 2655–2680 (1992).

6. T. Nakai and C. A. McDowell, An analysis of NMR spinning side-bands of homonuclear two-spin systems using Floquet theory, *Mol. Phys.* **77,** 569–584 (1992).

7. T. Nakai and C. A. McDowell, Application of Floquet theory to the nuclear magnetic resonance spectra of homonuclear two-spin systems in rotating solids, *J. Chem. Phys.* **96,** 3452–3466 (1992).

8. For general review articles on dipolar recoupling under MAS NMR conditions see (*i*) A. E. Bennett, R. G. Griffin, and S. Vega, Recoupling of homo- and heteronuclear dipolar interactions in rotating solids, *in* "Solid-State NMR IV: Methods and Applications of Solid-State NMR," Vol. 33, "NMR Basic Principles and Progress" (B. Blümich, Ed.), pp. 1–78, Springer-Verlag, Berlin (1994); (*ii*) S. Dusold and A. Sebald, Dipolar recoupling under magic-angle-spinning conditions, *in* "Annual Reports on NMR Spectroscopy" (G. Webb, Ed.), Vol. 41, pp. 185–264, Academic Press, London (2000), and references given there on methodology and applications of rotational-resonance NMR.

9. T. A. Early, B. K. John, and L. F. Johnson, Observation of homonuclear double-quantum correlations in plastic crystals using cross polarization and magic-angle spinning, *J. Magn. Reson.* **75,** 134–138 (1987).

10. R. Benn, H. Grondey, C. Brevard, and A. Pagelot, The detection of connectivities of rare spin-1/2 nuclei in the solid state using natural abundance samples: ^{13}C and ^{29}Si INADEQUATE and COSY type experiments, *J. Chem. Soc. Chem. Commun.*, 102–103 (1988); C. A. Fyfe, Y. Feng, H. Gies, H. Grondey, and G. T. Kokotailo, Natural-abundance solid-state ^{29}Si NMR investigations of three-dimensional lattice connectivities in zeolite structures, *J. Am. Chem. Soc.* **112,** 3264–3270 (1990).

11. I. D. Gay, C. H. W. Jones, and R. D. Sharma, INADEQUATE in the solid state. Homonuclear couplings in [(CH$_3$)$_2$SnE]$_3$, *J. Magn. Reson.* **91,** 186–189 (1991).

12. R. Challoner and A. Sebald, A double-quantum ^{119}Sn rotational-resonance study, *J. Magn. Reson. A* **122,** 85–89 (1996).

13. A. Lesage, C. Auger, S. Caldarelli, and L. Emsley, Determination of through-bond carbon–carbon connectivities in solid-state NMR using the INADEQUATE experiment, *J. Am. Chem. Soc.* **119,** 7867–7868 (1997); A. Lesage, M. Bardet, and L. Emsley, Through-bond carbon–carbon connectivities in disordered solids by NMR, *J. Am. Chem. Soc.* **121,** 10987–10993 (1999).

14. R. Verel, J. van Beek, and B. H. Meier, INADEQUATE-CR experiments in the solid state, *J. Magn. Reson.* **140,** 300–303 (1999).

15. T. Karlsson, M. Edén, H. Luthman, and M. H. Levitt, Efficient double-quantum excitation in rotational resonance NMR, *J. Magn. Reson.* **145,** 95–107 (2000).

16. W. Rach, G. Kiel, and G. Gattow, Untersuchungen über Salze der Pyruvinsäure. 2. Kristallstruktur von Kaliumpyruvat, Neubestimmung der Struktur von Natriumpyruvat, *Z. Anorg. Allg. Chem.* **563,** 87–95 (1988).

17. A. F. Pieret, F. Durant, M. Griffé, G. Germain, and T. Debaerdemaeker, Structure Cristalline de l'ester ethylique de la tyrosine, *Acta Crystallogr. B* **26,** 2117–2123 (1970).

18. A. E. Bennett, C. M. Rienstra, M. Auger, K. V. Lakshmi, and R. G. Griffin, Heteronuclear decoupling in rotating solids, *J. Chem. Phys.* **103,** 6951–6958 (1995).

19. M. H. Levitt, The signs of frequencies and phases in NMR, *J. Magn. Reson.* **126,** 164–182 (1997).

20. U. Haeberlen, High resolution NMR in solids. Selective averaging, *in* "Advances in Magnetic Resonance" (J. S. Waugh, Ed.), Supplement 1, Academic Press, New York (1976).

21. A. R. Edmonds, "Angular Momentum in Quantum Mechanics," Princeton Univ. Press, Princeton (1974).

22. S. Dusold, W. Milius, and A. Sebald, Iterative lineshape fitting of MAS NMR spectra: A tool to investigate homonuclear J couplings in isolated spin pairs, *J. Magn. Reson.* **135,** 500–513 (1998).

23. S. Dusold, H. Maisel, and A. Sebald, Magnitudes and orientations of interaction tensors determined from rotational resonance MAS NMR lineshapes of a four-^{13}C spin system, *J. Magn. Reson.* **141,** 78–90 (1999).

24. M. Bak and N. C. Nielsen, REPULSION, a novel approach to

efficient powder averaging in solid-state NMR, *J. Magn. Reson.* **125,** 132–139 (1997).

25. M. Edén and M. H. Levitt, Computation of orientational averages in solid state NMR by Gaussian spherical quadrature, *J. Magn. Reson.* **132,** 220–239 (1998).

26. S. A. Smith, T. O. Levante, B. H. Meier, and R. R. Ernst, Computer simulations in magnetic resonance. An object oriented programming approach, *J. Magn. Reson. A* **106,** 75–105 (1994).

27. M. Edén, Y. K. Lee, and M. H. Levitt, Efficient simulation of periodic problems in NMR: Application to decoupling and rotational resonance, *J. Magn. Reson. A* **120,** 56–71 (1996).

28. T. Charpentier, C. Fermon, and J. Virlet, Efficient time propagation technique for MAS NMR simulation: Application to quadrupolar nuclei, *J. Magn. Reson.* **132,** 181–190 (1998).

29. M. Hohwy, H. Bildsoe, H. J. Jakobsen, and N. C. Nielsen, Efficient spectral simulations in NMR of rotating solids. The γ-COMPUTE algorithm, *J. Magn. Reson.* **136,** 6–14 (1999).

30. M. H. Levitt and M. Edén, Numerical simulation of periodic NMR problems: Fast calculation of carousel averages, *Mol. Phys.* **95,** 879–890 (1998).

31. M. Bechmann, S. Dusold, and A. Sebald, to be published.

32. X. Helluy and A. Sebald, to be published.

33. D. P. Raleigh, F. Creuzet, S. K. Gupta, M. H. Levitt, and R. G. Griffin, Measurement of internuclear distances in polycrystalline solids: Rotationally enhanced transfer of nuclear spin magnetization, *J. Am. Chem. Soc.* **111,** 4502–4503 (1989).

34. P. R. Costa, B. Sun, and R. G. Griffin, Rotational resonance tickling: Accurate internuclear distance measurements in solids, *J. Am. Chem. Soc.* **119,** 10821–10830 (1997).

35. M. Baldus, M. Tomaselli, B. H. Meier, and R. R. Ernst, Broadband polarization-transfer experiments for rotating solids, *Chem. Phys. Lett.* **230,** 329–336 (1994).

36. M. Baldus and B. H. Meier, Broadband polarization transfer under magic-angle spinning: Application to total through-space-correlation NMR spectroscopy, *J. Magn. Reson.* **128,** 172–193 (1997).